

J. Plasma Phys. (2022), vol. 88, 905880615 © The Author(s), 2022. Published by Cambridge University Press doi:10.1017/S0022377822001222

Density jump for oblique collisionless shocks in pair plasmas: allowed solutions

Antoine Bret ¹,2,† and Ramesh Narayan^{3,4}

¹ETSI Industriales, Universidad de Castilla-La Mancha, 13071 Ciudad Real, Spain
²Instituto de Investigaciones Energéticas y Aplicaciones Industriales, Campus Universitario de Ciudad Real, 13071 Ciudad Real, Spain

³Center for Astrophysics – Harvard and Smithsonian, Harvard University, 60 Garden Street, Cambridge, MA 02138, USA

⁴Black Hole Initiative at Harvard University, 20 Garden Street, Cambridge, MA 02138, USA

(Received 29 July 2022; revised 23 November 2022; accepted 23 November 2022)

Shock waves in plasma are usually dealt with using magnetohydrodynamics (MHD). Yet, MHD entails the assumption of a short mean free path, which is not fulfilled in a collisionless plasma. Recently, for pair plasmas, we devised a model allowing one to account for kinetic effects within a MHD-like formalism. Its relies on an estimate of the anisotropy generated when crossing the front, with a subsequent assessment of the stability of this anisotropy in the downstream. We solved our model for parallel, perpendicular and switch-on shocks. Here we bridge between all these cases by treating the problem of an arbitrarily, but coplanar, oriented magnetic field. Even though the formalism presented is valid for anisotropic upstream temperatures, only the case of a cold upstream is solved. We find extra solutions which are not part of the MHD catalogue, and a density jump that is notably less in the quasi-parallel, highly magnetized, regime. Given the complexity of the calculations, this work is mainly devoted to the presentation of the mathematical aspect of our model. A forthcoming article will be devoted to the physics of the shocks here defined.

Key words: astrophysical plasmas, plasma nonlinear phenomena, space plasma physics

1. Introduction

Shock waves in plasmas are typically analysed using the tools of magnetohydrodynamics (MHD). Hence, the jump conditions derived rely on two assumptions: (1) that collisions are frequent enough to establish an isotropic pressure, both upstream and downstream, and (2) that all the matter upstream passes to the downstream, together with the momentum and the energy it carries (Gurnett & Bhattacharjee (2005), § 5.4.4; Goedbloed, Keppens & Poedts (2010) chapters 2 and 3; or Thorne & Blandford (2017), § 13.2).

It turns out that in collisionless plasmas, where the mean free path is much larger than the size of the system, shock front included, these two assumptions may not be fulfilled. Regarding the second one, it has been known for long that collisionless shocks can accelerate particles which escape the 'Rankine–Hugoniot budget' and modify the jump

† Email address for correspondence: antoineclaude.bret@uclm.es

conditions (Berezhko & Ellison 1999). As for the first assumption, namely that pressures are isotropic, it is still valid in collisionless unmagnetized plasmas since, in such plasmas, the Weibel instability ensures isotropic pressures are unstable (Weibel 1959; Silva, Afeyan & Silva 2021).

Yet, still in a collisionless plasma, an external magnetic field can stabilize an anisotropy, invalidating the second assumption (Hasegawa 1975; Gary 1993). This has been clearly proved by *in situ* measurement in the solar wind (Bale *et al.* 2009; Maruca, Kasper & Bale 2011; Schlickeiser *et al.* 2011). The present work is about departures from MHD predictions stemming from the violation of the second assumption. Departures stemming from the violation of the first one, namely accelerated particles escaping the Rankine–Hugoniot budget, will not be addressed here (see Bret (2020) for a review).

Assuming an isotropic upstream, how could any anisotropy develop downstream? Simply through an anisotropy that would be triggered at the front crossing, and then maintained stable in the downstream by means of an external magnetic field. Such is the scenario we have been contemplating in a series of recent articles on parallel, perpendicular and switch-on shocks (Bret & Narayan 2018, 2019, 2020, 2022).

In our model, the plasma is compressed anisotropically when it crosses the front. Then, depending on the resulting anisotropy degree, the field can sustain the anisotropy in the downstream, or not. Note that for the parallel case, our model has been successfully tested against particle-in-cell (PIC) simulations in Haggerty, Bret & Caprioli (2022).

The present work aims at bridging between all the previously treated cases. We therefore consider the general case of an oblique shock, where the upstream magnetic field makes an arbitrary angle with the shock normal.

The system considered is pictured in figure 1. Subscripts '1' and '2' refer to the upstream and the downstream respectively. We work in the reference frame where the upstream velocity v_1 is normal to the front. The upstream magnetic field B_1 makes an arbitrary angle $\theta_1 \neq 0$ with the shock normal, contrary to Bret & Narayan (2018, 2022) where $\theta_1 = 0$, and to Bret & Narayan (2019) where $\theta_1 = \pi/2$. The fields $B_{1,2}$ and the velocities $v_{1,2}$ are assumed coplanar.

Even though the formalism presented is valid for anisotropic downstream and upstream temperatures, we restrict ourselves to $T_{1\parallel} = T_{1\perp} = 0$ when solving it.

Also, we consider a plasma of electron–positron pairs. The identity of the mass of both species allows us to deal with only one parallel and one perpendicular temperature in the downstream, as it has been found that in collisionless shocks, species of different mass are heated differently (Feldman *et al.* 1982; Guo, Sironi & Narayan 2017, 2018).

As the reader will realize, even for a coplanar geometry with $T_{1\parallel} = T_{1\perp} = 0$, the forthcoming algebra is quite involved. For this reason, the present work is mainly devoted to the algebraic resolution of our model for the oblique case. We write down the conservation equations and explain how to solve them symbolically. We also explain how these solutions fit with each other within the rules of our model. Yet, as known even for MHD, listing the solutions of the equations does not provide the full picture of the shock physics, as some solutions which do satisfy the MHD conservation equations could eventually be non-physical (Kennel, Blandford & Wu 1990; Falle & Komissarov 1997; Wu 2003; Kulsrud 2005; Goedbloed 2008; Delmont & Keppens 2011). An assessment of the physical relevance of our solutions will be presented in a forthcoming article. Here, we focus on the mathematical solutions of our model.

This article is structured as follows. In § 2, we explain our model, emphasizing how we bridge between our previous treatments of the parallel and the perpendicular cases. In particular, we introduce 'Stage 1' and 'Stage 2' which are supposed to be two stages of the kinetic history of the plasma. In § 3, we introduce the conservation equations for

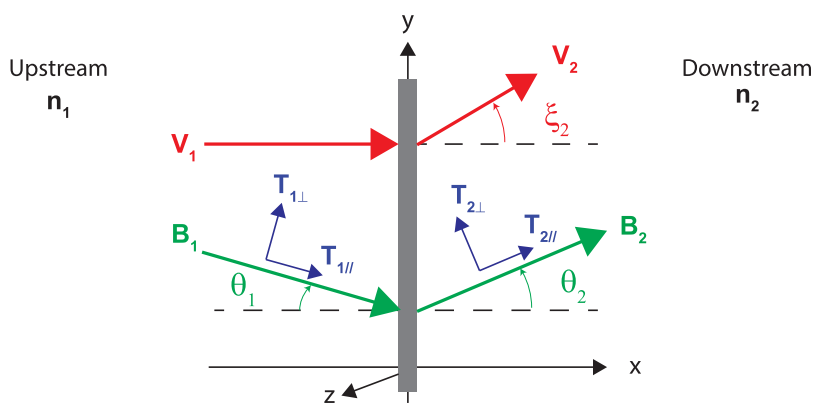


FIGURE 1. System considered. The upstream magnetic field \mathbf{B}_1 makes an angle θ_1 with the shock normal. The downstream field \mathbf{B}_2 and velocity \mathbf{v}_2 make angles θ_2 and ξ_2 respectively with the shock normal. We work in the reference frame where the shock is stationary and the upstream velocity \mathbf{v}_1 is normal to the front ($\xi_1=0$). The upstream has density n_1 and temperatures $T_{1\parallel}$ and $T_{1\perp}$ parallel and perpendicular to the upstream field \mathbf{B}_1 . The downstream has density n_2 and temperatures $T_{2\parallel}$ and $T_{2\perp}$ parallel and perpendicular to the downstream field \mathbf{B}_2 . The parallel and perpendicular directions are therefore defined with respect to the local magnetic field. Even though the equations presented in § 3 can be applied to an anisotropic upstream, the model is only solved for $T_{1\parallel}=T_{1\perp}=0$.

anisotropic temperatures, together with the dimensionless variables used subsequently. In §§ 4, 5 and 6, Stages 1 and 2 are studied separately. Then in § 7, we explain how they relate to each other in order to fully characterize the shock within our model for any field obliquity θ_1 .

2. Method

Although the method used to deal with the oblique case has been explained in Bret & Narayan (2022), we here outline it for completeness.

Consider an upstream with temperatures $T_{1\parallel}$ and $T_{1\perp}$. If the crossing of the front could be fully described by the isentropic Vlasov equation (Landau & Lifshitz 1981, § 27), the downstream temperatures could be related to the other quantities through the expressions derived in Chew, Goldberger & Low (1956):

$$T_{2\parallel} = T_{1\parallel} \left(\frac{n_2 B_1}{n_1 B_2} \right)^2,$$

$$T_{2\perp} = T_{1\perp} \frac{B_1}{B_2}.$$
(2.1)

But the crossing of the front is not isentropic since in a shock there is an entropy increase from the upstream to the downstream. As a consequence, temperatures increase by more than the amount specified by (2.1), as found in the PIC simulations of Haggerty *et al.* (2022). In both the parallel case ($\theta_{1,2} = 0$) and the perpendicular case ($\theta_{1,2} = \pi/2$), we considered this excess goes into the temperature parallel to the motion, since the compression at the front can be considered to operate along this direction. As a consequence, the temperature parallel to the motion increases, while the temperature perpendicular to the motion remains constant.

Hence, denoting T_{entropy} as the temperature correction due to entropy generation, we took for the parallel case

$$T_{2\parallel} = T_{1\parallel} \left(\frac{n_2 B_1}{n_1 B_2} \right)^2 + T_{\text{entropy}},$$

$$T_{2\perp} = T_{1\perp} \frac{B_1}{B_2}$$
(2.2)

and for the perpendicular case

$$T_{2\parallel} = T_{1\parallel} \left(\frac{n_2 B_1}{n_1 B_2}\right)^2,$$

$$T_{2\perp} = T_{1\perp} \frac{B_1}{B_2} + T_{\text{entropy}}.$$
(2.3)

In order to bridge between these two extremes, we now make the following ansatz:

$$T_{2\parallel} = T_{1\parallel} \left(\frac{n_2 B_1}{n_1 B_2} \right)^2 + T_e \cos^2 \theta_2, \tag{2.4}$$

$$T_{2\perp} = T_{1\perp} \frac{B_1}{B_2} + \frac{1}{2} T_e \sin^2 \theta_2, \tag{2.5}$$

where T_e (subscript e for entropy) will be determined by the conservation equations.

Physically, (2.4) and (2.5) are motivated by our hypothesis that the excess energy goes into a direction parallel to the upstream velocity, by analogy with our previous treatments of the parallel and perpendicular shock subcases. Geometry is then used to divide the energy excess between $T_{2\parallel}$ and $T_{2\perp}$.

The scheme chosen in (2.4) and (2.5) is the simplest one fulfilling the following conditions:

- (i) It correctly reduces to (2.2) and (2.3) for $\theta_2 = 0$ and $\theta_2 = \pi/2$.
- (ii) All temperature excesses sum up to T_e .
- (iii) It guaranties the two downstream temperatures normal to the field B_2 are equal, which is required by the Vlasov equation (Landau & Lifshitz 1981, § 53).

Its relevance will have to be checked via PIC simulation, like that of Bret & Narayan (2018) has been checked in Haggerty *et al.* (2022).

The downstream temperatures after the front crossing are therefore given by (2.4) and (2.5). We refer to this state of the downstream as 'Stage 1'. Depending of the strength of the downstream field B_2 , Stage 1 can be stable or unstable.

Previous analysis showed that Stage 1 can be firehose or mirror unstable. In the case where Stage 1 is firehose unstable, it migrates to the 'Stage-2-firehose' state, on the firehose instability threshold where (Hasegawa 1975; Gary 1993; Gary & Karimabadi 2009)

$$A_2 \equiv \frac{T_{2\perp}}{T_{2\parallel}} = 1 - \frac{1}{\beta_{2\parallel}},$$
 (2.6)

with

$$\beta_{2\parallel} = \frac{n_2 k_B T_{2\parallel}}{B_2^2 / 4\pi},\tag{2.7}$$

Upstream	Downstream in Stage 1	Stable?	End state of the downstream
$T_{1\parallel}=T_{1\perp}=0$	$T_{2\perp}$ and $T_{2\parallel}$ given by (2.4) and (2.5)	Stable \rightarrow Firehose unstable \rightarrow Mirror unstable \rightarrow	Stage 1 Stage-2-firehose Stage-2-mirror

TABLE 1. Summary of the assumed kinetic history of the plasma as it crosses the front. Although the formalism presented in § 3 allows for an anisotropic upstream, the model is only solved for $T_{1\parallel} = T_{1\perp} = 0$.

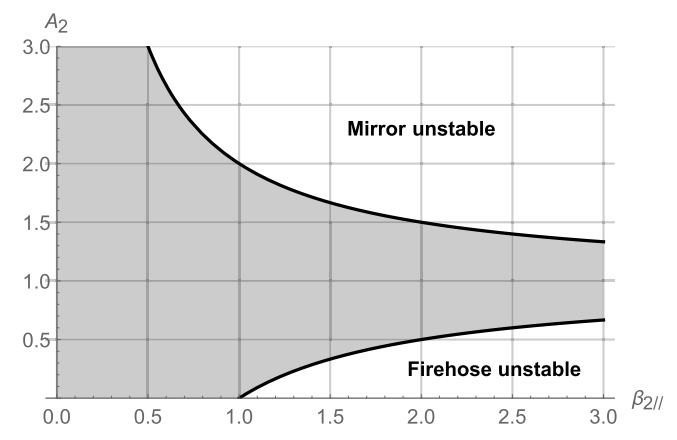


FIGURE 2. Instability thresholds (2.6) and (2.8) for the firehose and mirror instabilities. The system is stable in the shaded region and the instability domains do not overlap.

where k_B is the Boltzmann constant. In the case where Stage 1 is mirror unstable, it migrates to the 'Stage-2-mirror' state, on the mirror instability threshold where

$$A_2 = 1 + \frac{1}{\beta_{2\parallel}}. (2.8)$$

At any rate, imposing condition (2.6) or (2.8) in the forthcoming conservation equations determines the state of the downstream. Our algorithm is summarized in table 1.

The firehose instability reaches its maximum growth rate for k parallel to the field, while the mirror instability reaches its maximum growth rate for a k making an oblique angle with the field (Gary 1993, § 7.2). The instability thresholds (2.6) and (2.8) for the firehose and mirror instabilities are plotted in figure 2. Of note, the instability domains do not overlap in the $(\beta_{2\parallel}, A_2)$ plane so that the two instabilities cannot compete with each other.

3. Conservation equations

The conservation equations for anisotropic temperatures were derived in Hudson (1970), Erkaev, Vogl & Biernat (2000) and Génot (2009). They have been re-derived in Bret &

Narayan (2022) with the present notations. They are formally valid even for anisotropic upstream temperatures, with $T_{1\parallel} \neq T_{1\perp}$. Writing them for $T_{1\parallel} = T_{1\perp} \equiv T_1$, they read

$$n_2 v_2 \cos \xi_2 = n_1 v_1, \tag{3.1}$$

$$B_2 \cos \theta_2 = B_1 \cos \theta_1, \tag{3.2}$$

$$B_2 v_2 \sin \theta_2 \cos \xi_2 - B_2 v_2 \cos \theta_2 \sin \xi_2 = B_1 v_1 \sin \theta_1, \tag{3.3}$$

$$\frac{B_2^2 \sin^2 \theta_2}{8\pi} + n_2 k_B (T_{\parallel 2} \cos^2 \theta_2 + T_{\perp 2} \sin^2 \theta_2) + m n_2 v_2^2 \cos^2 \xi_2$$

$$=\frac{B_1^2 \sin^2 \theta_1}{8\pi} + n_2 k_B T_1 + m n_1 v_1^2,\tag{3.4}$$

$$A + mn_2 v_2^2 \sin \xi_2 \cos \xi_2 = -\frac{B_1^2 \sin \theta_1 \cos \theta_1}{4\pi},$$
(3.5)

$$Av_2 \sin \xi_2 + B + C = mn_1 v_1 \left(\frac{5k_B T_1}{2m} + \frac{B_1^2 \sin^2 \theta_1}{4\pi m n_1} + \frac{v_1^2}{2} \right), \tag{3.6}$$

where

$$\mathcal{A} = \sin \theta_{2} \cos \theta_{2} n_{2} k_{B} \left(T_{\parallel 2} - T_{\perp 2} \right) - \frac{B_{2}^{2}}{4\pi} \sin \theta_{2} \cos \theta_{2},$$

$$\mathcal{B} = v_{2} \cos^{2} \theta_{2} \cos \xi_{2} n_{2} k_{B} (T_{\parallel 2} - T_{\perp 2}),$$

$$\mathcal{C} = m n_{2} v_{2} \cos \xi_{2} \left(\frac{k_{B}}{2m} (T_{\parallel 2} + 4T_{\perp 2}) + \frac{B_{2}^{2} \sin^{2} \theta_{2}}{4\pi m n_{2}} + \frac{v_{2}^{2}}{2} \right).$$
(3.7)

The anisotropic upstream version of these equations is obtained by replacing the right-hand side of each equation by the left-hand side, changing subscripts '2' to '1' and then setting $\xi_1 = 0$. Indeed, in the case where a shock propagates behind another one, the downstream of the first shock is eventually the upstream of the next one. A formalism accounting for an anisotropic upstream is therefore necessary since our model always leaves an anisotropic downstream (unless $B_1 = 0$).

Even though the model can be solved, the algebra is extremely involved. The system is symbolically solved with Mathematica. Its solutions are then numerically studied in MATLAB. On occasions, the Mathematica calculations give rise to the resolution of a polynomial of considerable length. In such cases, the polynomial is transferred to MATLAB using the Mathematica Notebook described in Bret (2010).

It is useful to focus on the quantity

$$T2 \equiv \tan \theta_2,\tag{3.8}$$

as the system of equations above allows one to deduce a polynomial equation for T2, easy to solve numerically. The general pattern of the resolution consists therefore of deriving such a polynomial and, from its roots, to compute the other downstream quantities like n_2 , in terms of the upstream parameters.

The following dimensionless variables are used throughout this work:

$$r = \frac{n_2}{n_1}, \quad \mathcal{M}_{A1} = \sqrt{\frac{mn_1v_1^2}{B_1^2/4\pi}}, \quad \sigma = \frac{B_1^2/4\pi}{mn_1v_1^2} = \frac{1}{\mathcal{M}_{A1}^2}.$$
 (3.9*a-c*)

While the Alfvén Mach number $\mathcal{M}_{A,i}$ is prominent in the shock literature, the related σ parameter is typically used in PIC simulations like those of Haggerty *et al.* (2022).

In order to simplify the problem, in the present work we restrict ourselves to the case $T_1 = 0$, that is, the strong sonic shock case. This is why no sonic Mach number is defined above.

The upstream is therefore characterized by four variables: n_1 , θ_1 , B_1 and v_1 . The downstream is characterized by six variables: n_2 , θ_2 , B_2 , v_2 , ξ_2 and T_e . The six equations (3.1)–(3.6) then allow one to solve the problem.

We now outline the resolution of the conservation equations for Stage 1, Stage-2-firehose and Stage-2-mirror.

4. Study of Stage 1

With $T_{1\parallel} = T_{1\perp} = 0$, (2.4) and (2.5) for Stage 1 read

$$T_{2\parallel} = T_e \cos^2 \theta_2, T_{2\perp} = \frac{1}{2} T_e \sin^2 \theta_2.$$
(4.1)

4.1. Symmetries

Although not immediately visible, the system (3.1)–(3.6) with prescriptions (4.1) has some symmetries.

It can be checked that, all other things being equal, if the set of angles $(\theta_1, \theta_2, \xi_2)$ is a solution, then $(-\theta_1, -\theta_2, -\xi_2)$ is also a solution, while $(-\theta_1, +\theta_2, \pm \xi_2)$ is not. This implies that we cannot ignore the negative θ_2 . We then restrict our exploration to $\theta_1 \in [0, \pi/2]$ and solve for $\theta_2, \xi_2 \in [-\pi/2, \pi/2]$.

4.2. Resolution

Resolving Stage 1 is then achieved through the following steps:

- (i) Eliminate v_2 everywhere by extracting its value from (3.1).
- (ii) Eliminate B_2 everywhere by extracting its value from (3.2).
- (iii) Use the resulting (3.4) to eliminate T_e .
- (iv) At this juncture, we are left with n_2 , θ_2 and ξ_2 as unknowns. Parameter ξ_2 can be eliminated (defining $X2 \equiv \tan \xi_2$). We finally obtain two equations for $r = n_2/n_1$ and $T2 = \tan \theta_2$.

The equation for T2 reads

$$(T2\cos\theta_1 - \sin\theta_1)\underbrace{\sum_{k=0}^{9} a_k T2^k}_{=A} = 0,$$
 (4.2)

with

$$a_{0} = -128 \left(-2\mathcal{M}_{A1}^{2} + \cos(2\theta_{1}) + 1\right)^{2} \sin \theta_{1},$$

$$a_{1} = 128 \cos \theta_{1} \left(4\mathcal{M}_{A1}^{4} - 2\mathcal{M}_{A1}^{2} + \left(2 - 6\mathcal{M}_{A1}^{2}\right) \cos(2\theta_{1}) + \cos(4\theta_{1}) + 1\right),$$

$$a_{2} = -16 \left(16\mathcal{M}_{A1}^{4} - 16\mathcal{M}_{A1}^{2} + \left(8 - 16\mathcal{M}_{A1}^{2}\right) \cos(2\theta_{1}) + \cos(4\theta_{1}) + 7\right) \sin \theta_{1},$$

$$a_{3} = 8 \cos \theta_{1} \left(16\mathcal{M}_{A1}^{4} - 44\mathcal{M}_{A1}^{2} + \left(48 - 68\mathcal{M}_{A1}^{2}\right) \cos(2\theta_{1}) + 17 \cos(4\theta_{1}) + 31\right),$$

$$a_{4} = 4 \left(-32\mathcal{M}_{A1}^{4} + 40 \cos(2\theta_{1})\mathcal{M}_{A1}^{2} + 40\mathcal{M}_{A1}^{2} + \cos(4\theta_{1}) - 1\right) \sin \theta_{1},$$

$$a_{5} = 4 \cos \theta_{1} \left(-16 \left(2\mathcal{M}_{A1}^{4} + \mathcal{M}_{A1}^{2}\right) + 8 \left(7 - 2\mathcal{M}_{A1}^{2}\right) \cos(2\theta_{1}) + 15 \cos(4\theta_{1}) + 41\right),$$

$$a_{6} = -2 \left(96\mathcal{M}_{A1}^{4} - 112\mathcal{M}_{A1}^{2} + 8 \left(3 - 14\mathcal{M}_{A1}^{2}\right) \cos(2\theta_{1}) + 9 \cos(4\theta_{1}) + 15\right) \sin \theta_{1},$$

$$a_{7} = 2 \cos \theta_{1} \left(32\mathcal{M}_{A1}^{4} + 16\mathcal{M}_{A1}^{2} + 8 \left(5 - 6\mathcal{M}_{A1}^{2}\right) \cos(2\theta_{1}) + 15 \cos(4\theta_{1}) + 25\right),$$

$$a_{8} = 16 \cos^{4} \theta_{1} \sin \theta_{1},$$

$$a_{9} = 16 \cos^{5} \theta_{1}.$$

$$(4.3)$$

The equation for r reads

$$r = \frac{4\mathcal{M}_{A1}^2 T 2^3 (1 + T 2^2)}{\sum_{k=0}^{5} b_k T 2^k},$$
(4.4)

where

$$b_{0} = 8\mathcal{M}_{A1}^{2} \tan \theta_{1} - 4\sin(2\theta_{1}),$$

$$b_{1} = -8\mathcal{M}_{A1}^{2} + 6\cos(2\theta_{1}) + 2,$$

$$b_{2} = 0,$$

$$b_{3} = 4\mathcal{M}_{A1}^{2} + \cos(2\theta_{1}) + 3,$$

$$b_{4} = 4\mathcal{M}_{A1}^{2} \tan \theta_{1} - 2\sin(2\theta_{1}),$$

$$b_{5} = 2\cos^{2}\theta_{1}.$$

$$(4.5)$$

Equation (4.2) is a polynomial yielding various T2 branches as solutions. Scanning them, and using (4.4), allows the derivation of the density jump. Note that one value of T2 gives one single value of r.

Equation (4.2) clearly displays two main branches:

- (i) $T2\cos\theta_1 \sin\theta_1 = 0$, that is, $\theta_2 = \theta_1$. Inserting in (4.4) gives r = 1. This is the continuity solution.
- (ii) $\Lambda = 0$. The values of the density ratio r so defined are represented in figure 3 in terms of (σ, θ_1) . For $\theta_1 = 0$, we recover the solutions found in Bret & Narayan (2018, 2022). For $\theta_1 = \pi/2$, we recover the solutions found in Bret & Narayan (2019).

All these Stage 1 solutions do not make their way to the end state of the downstream since some are unstable. We need now to assess the stability of Stage 1.

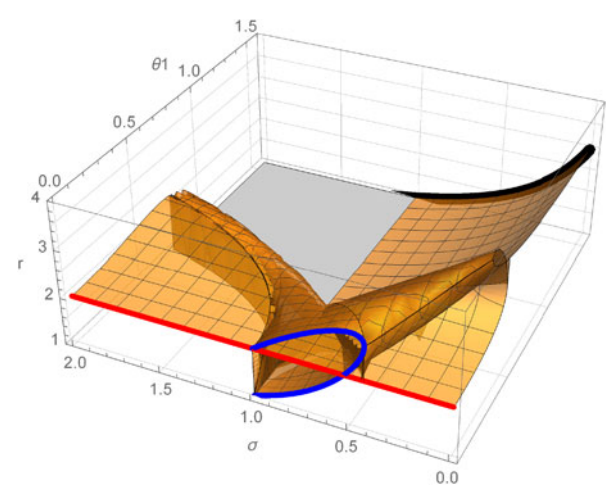


FIGURE 3. Values of the density ratio r for Stage 1, with θ_2 given by $\Lambda=0$ as defined by (4.2). The red curve was studied in Bret & Narayan (2018). The blue one was studied in Bret & Narayan (2022). The blue curve has $\theta_2 > 0$. The red one has $\theta_2 = 0$. The thick black curve at $\theta_1 = \pi/2$ was studied in Bret & Narayan (2019).

4.3. Stability of Stage 1

From (2.6) and (2.8), we see that assessing the stability of Stage 1 requires computing its anisotropy A_2 and its $\beta_{2\parallel}$ parameter. The anisotropy for Stage 1 is straightforwardly given by (4.1) as

$$A_2 = \frac{T_{2\perp}}{T_{2\parallel}} = \frac{1}{2} T_e \tan^2 \theta_2. \tag{4.6}$$

The $\beta_{\parallel 2}$ parameter is given by

$$\beta_{\parallel 2} = 2 \frac{\sec^2 \theta_1 \left(2\mathcal{M}_{A1}^2 (r-1) + r \right) - r \left(T2^2 + 1 \right)}{r \left(T2^4 + 2 \right)}.$$
 (4.7)

Using (4.6) and (4.7) we can then numerically assess the firehose or mirror instability of Stage 1. Depending on the result, Stage 1 will be the end state of the downstream, or else it will migrate to Stage-2-firehose or Stage-2-mirror, on the corresponding instability thresholds.

5. Study of Stage-2-firehose

In the case where Stage 1 is firehose unstable, it will migrate to the firehose stability threshold. In order to determine its properties, we need now to impose condition (2.6) to the system (3.1)–(3.6) instead of the temperature prescriptions (4.1).

The resolution strategy is similar to that for Stage 1. Now $T2 = \tan \theta_2$ is given solving

$$\sum_{k=0}^{4} a_k T 2^k = 0, (5.1)$$

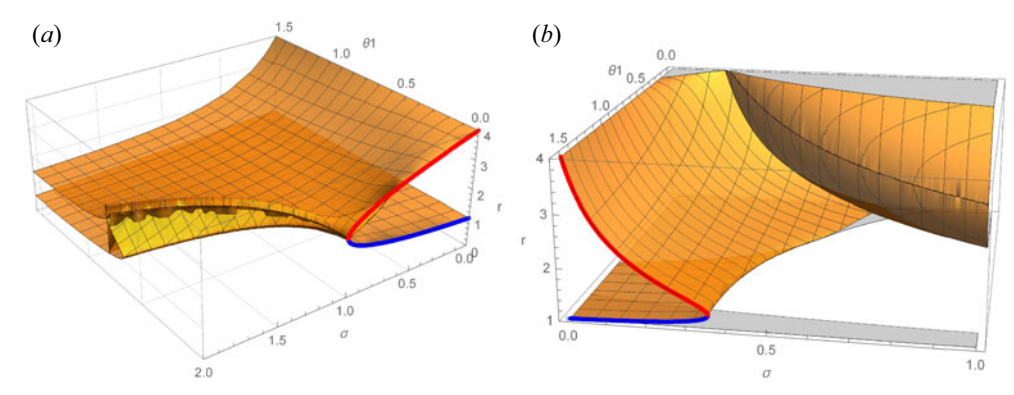


FIGURE 4. (a) Values of r for Stage-2-firehose, where θ_2 is given by (5.1). The blue and red curves were studied in Bret & Narayan (2018). The blue one has temperature anisotropy $A_2 < 0$ and is therefore non-physical. (b) Values of r for Stage-2-mirror. The blue and red curves were studied in Bret & Narayan (2019). The blue one has $A_2 < 0$.

with

$$a_{0} = -32 \left(\mathcal{M}_{A1} \sin(2\theta_{1}) - 2\mathcal{M}_{A1}^{3} \tan \theta_{1} \right)^{2},$$

$$a_{1} = -10\mathcal{M}_{A1}^{2} \left[\left(20\mathcal{M}_{A1}^{2} - 2 \right) \sin(2\theta_{1}) - 8 \left(2\mathcal{M}_{A1}^{2} + 1 \right) \tan \theta_{1} \mathcal{M}_{A1}^{2} - 3 \sin(4\theta_{1}) \right],$$

$$a_{2} = \mathcal{M}_{A1}^{2} \left[-32\mathcal{M}_{A1}^{4} + 8\mathcal{M}_{A1}^{2} + 24 \left(3\mathcal{M}_{A1}^{2} - 1 \right) \cos(2\theta_{1}) - 15 \cos(4\theta_{1}) - 9 \right],$$

$$a_{3} = 0,$$

$$a_{4} = -8\mathcal{M}_{A1}^{2} \cos^{4} \theta_{1}.$$
(5.2)

Then the density jump reads

$$r = \frac{2\mathcal{M}_{A1}^2 T2}{-\sin(2\theta_1) + 2\mathcal{M}_{A1}^2 \tan\theta_1 + T2\cos^2\theta_1}.$$
 (5.3)

Again, one value of T2 corresponds to one and only one value of r.

The density jump so defined is plotted in figure 4(a) in terms of (σ, θ_1) . For $\theta_1 = 0$, the red arc joining $(\sigma = 0, r = 4)$ to $(\sigma = 1, r = 2)$ fits exactly what was found in Bret & Narayan (2018). In Bret & Narayan (2018), we argued that the blue arc, joining $(\sigma = 0, r = 1)$ to $(\sigma = 1, r = 2)$, was not a shock solution since it reaches r = 1 for $\sigma = 0$. In fact, these blue solutions are discarded on an even simpler physical ground: they have $A_2 < 0$. For Stage-2-firehose, the anisotropy is no longer given by (4.6) but by

$$A_2 = 1 - \frac{r(T2^2 + 1)\cos^2\theta_1}{2\mathcal{M}_{A1}^2(r - 1) + r\sin^2\theta_1}.$$
 (5.4)

When computing this quantity for the lower, blue arc, and indeed for the whole lower surface in figure 4(a), $A_2 < 0$ is found. This property will be useful when putting Stages 1 and 2 together in § 7.

6. Study of Stage-2-mirror

If Stage 1 is mirror unstable we need to impose relation (2.8) to the conservation equations. The quantity T2 is still a solution of the polynomial equation (5.1), where the

coefficients are now

$$a_{0} = 4\left(\sin(2\theta_{1}) - 2\mathcal{M}_{A1}^{2} \tan\theta_{1}\right)^{2},$$

$$a_{1} = \frac{1}{4}\left[2\left(74\mathcal{M}_{A1}^{2} - 17\right)\sin(2\theta_{1}) - 40\left(2\mathcal{M}_{A1}^{2} + 1\right)\tan\theta_{1}\mathcal{M}_{A1}^{2} - 27\sin(4\theta_{1})\right],$$

$$a_{2} = 4\mathcal{M}_{A1}^{4} + 8\sin^{2}\theta_{1}\mathcal{M}_{A1}^{2} + 30\cos^{4}\theta_{1} - \cos^{2}\theta_{1}\left(30\mathcal{M}_{A1}^{2} + 19\sin^{2}\theta_{1}\right),$$

$$a_{3} = -\left(1 - 2\mathcal{M}_{A1}^{2} + \cos(2\theta_{1})\right)\sin(2\theta_{1}),$$

$$a_{4} = 15\cos^{4}\theta_{1}.$$

$$(6.1)$$

Then the density jump becomes

$$r = \frac{2\mathcal{M}_{A1}^2 T2}{-\sin(2\theta_1) + 2\mathcal{M}_{A1}^2 \tan \theta_1 + 3T2\cos^2 \theta_1}.$$
 (6.2)

The results are plotted in figure 4(b) in terms of (σ, θ_1) . A pattern similar to that of Stage-2-firehose emerges here. When treating the $\theta_1 = \pi/2$ problem in Bret & Narayan (2019), we discarded the lower branch in blue at $\theta_1 = \pi/2$, arguing that it is not a shock solution since it reaches r = 1 for $\sigma = 0$. It turns out that this branch again has anisotropy $A_2 < 0$. For Stage-2-mirror, this quantity reads

$$A_2 = -\frac{-4\mathcal{M}_{A1}^2(r-1) + rT2^2\cos(2\theta_1) + r\left(T2^2 - 2\right)}{4\mathcal{M}_{A1}^2(r-1) - r\left(2T2^2 + 1\right)\cos(2\theta_1) - 2rT2^2 + r},$$
(6.3)

and is found negative on the blue arc in figure 4(b), as well as along the lower surface that extends from this arc.

7. Putting Stages 1 and 2 together

We finally come to the point where we can assemble Stages 1 and 2. This has been performed in MATLAB according to the following algorithm:

- (a) Solve $\Lambda = 0$ in (4.2) for T2 in Stage 1, and record all the branches of the solutions.
- (b) Then scan each Stage 1 branch. If a Stage 1 state is found stable, then this is the end state of the downstream.
- (c) If a Stage 1 state is found firehose unstable, then switch to Stage-2-firehose, end state of the downstream.
- (d) If a Stage 1 state is found mirror unstable, then switch to Stage-2-mirror, end state of the downstream.

Steps (c) and (d) can be non-trivial when, for an unstable Stage 1 state (σ, θ_1) , there are more than one Stage 2 states with the same (σ, θ_1) . Some criteria are needed in order to select one Stage 2 state among the possible solutions. We apply the following ones:

- (a) Discard Stage 2 states with $A_2 < 0$ since they represent non-physical solutions to the equations.
- (b) In the case where degeneracy persists, select the Stage 2 state which has θ_2 closest to the unstable Stage 1.

We now check how this method retrieves our previous result, before applying it to any intermediate angle θ_1 .

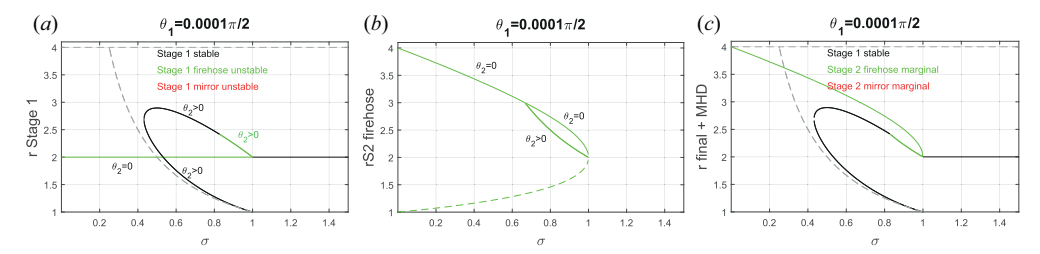


FIGURE 5. (a) All solutions of Stage 1 for θ_1 close to zero, colour-coded according to their stability (none is mirror unstable). (b) All Stage-2-firehose solutions. Dashed line indicates $A_2 < 0$ (non-physical). (c) End result. The grey dashed lines show the MHD solutions.

7.1. *Case*
$$\theta_1 \sim 0$$

The case $\theta_1 \sim 0$ is pictured in figure 5. Figure 5(a) shows all Stage 1 solutions. Black means they are stable, green means they are firehose unstable. Red would mean mirror unstable, but, for the selected θ_1 , there are no such cases. The solution r=2 has $\theta_1=\theta_2\sim 0$. It pertains to the parallel case which was studied in Bret & Narayan (2018). The other solutions, which draw an open loop, pertain to the switch-on case studied in Bret & Narayan (2022). They have $\theta_2>0$. These switch-on solutions are physical, namely they have $A_2>0$ (see figure 4a of Bret & Narayan 2022).

Figure 5(b) shows all solutions for Stage-2-firehose. We see that an unstable Stage 1 state with $\sigma=0.9$, for example, can in principle go to three Stage-2-firehose states. Out of these three, one has $A_2<0$, as indicated by the dashed line in figure 5(b). Among the two remaining options, the upper one has $\theta_2=0$ while the lower one has $\theta_2>0$. Therefore, choosing the Stage 2 state which has closest θ_2 to the unstable Stage 1, leaves only one possible option.

Figure 5(c) shows the end result. We recover the result of the parallel case, with a marginal firehose jump going from r=4 to 2 for $0<\sigma<1$, and then Stage 1 stable with r=2 for $\sigma>1$ (Bret & Narayan 2018). Also recovered are the two switch-on solutions found in Bret & Narayan (2022), with a portion of the upper one being replaced by its Stage-2-firehose counterpart.

7.2. Case
$$\theta_1 \sim \pi/2$$

We here check the conformity of the present calculations with the results previously derived in Bret & Narayan (2019) for the perpendicular case.

Figure 6(a) shows Stage 1 solutions. There is but one branch solution, mirror unstable for $\sigma < \sigma_c$, where $\sigma_c = 0.106$.

Figure 6(b) shows all Stage-2-mirror branches. There is but one, with $A_2 < 0$ below $r \sim 2.47$, which is reached for $\sigma = \sigma'_c$. We checked numerically, up to the 13th digit, that $\sigma_c = \sigma'_c$.

As a consequence, figure 6(c), which features the end result, has no gap. It fits exactly the result of Bret & Narayan (2019). For $\sigma < \sigma_c$, Stage 1 is mirror unstable and the end state is Stage-2-mirror. Then for $\sigma > \sigma_c$, Stage 1 is stable and gives the density jump of the end state.

7.3. General oblique case

Figure 7 pictures the situation for an intermediate angle $\theta_1 = 0.3\pi/2$. Figure 7(a) shows all of Stage 1 solutions. Here, some are mirror unstable while others are firehose unstable. Looking at figures 7(c) and 7(b) we can see that there is always a Stage 2 solution when

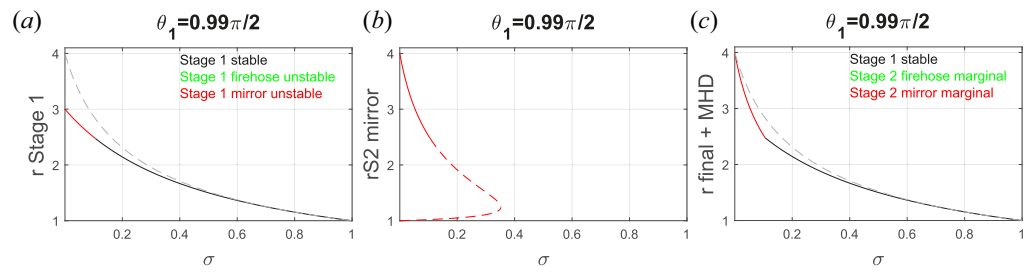


FIGURE 6. (a) All solutions of Stage 1 for θ_1 close to $\pi/2$, colour-coded according to their stability (none is firehose unstable). (b) All Stage-2-mirror solutions. Dashed line indicates A_2 < 0 (non-physical). (c) End result. The grey dashed lines show the MHD solutions.

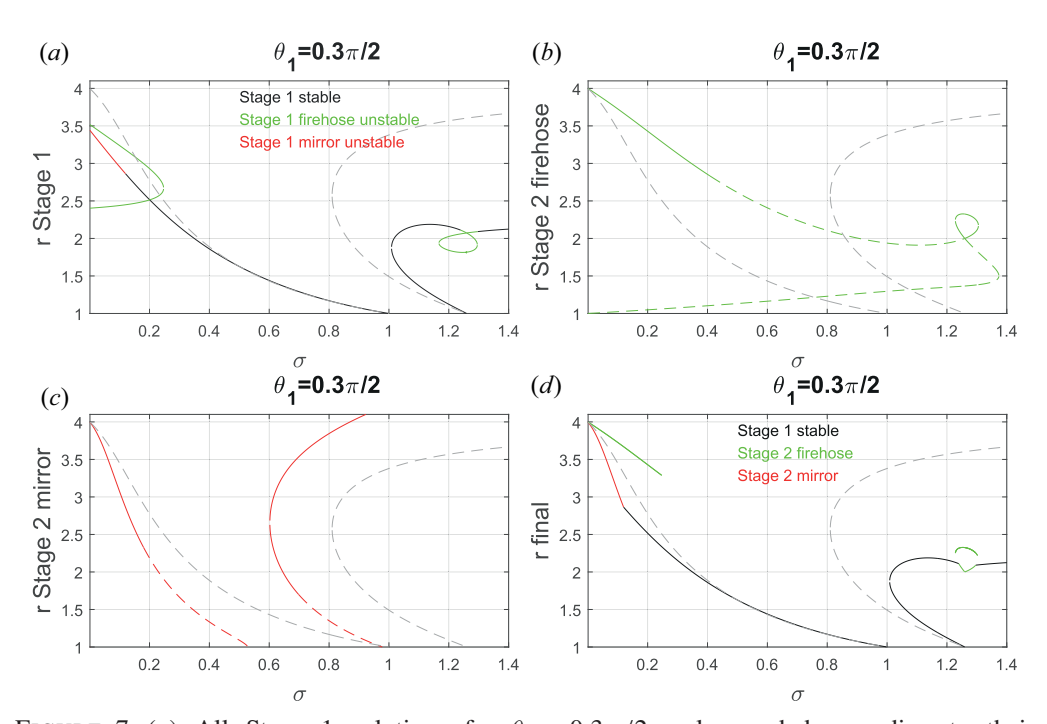


FIGURE 7. (a) All Stage 1 solutions for $\theta_1 = 0.3\pi/2$, colour-coded according to their stability. (b) All Stage-2-firehose solutions. Dashed line when $A_2 < 0$ (non-physical). (c) All Stage-2-mirror solutions. Dashed line when $A_2 < 0$ (non-physical). (d) End result. The grey dashed lines show the MHD solutions.

Stage 1 is unstable. For some values of σ , for example 0.1 or 1.25, there are various unstable Stage 1 solutions. As a consequence, figure 7(d) displays various solutions for the end state corresponding to these σ .

Notice also how our solutions mimic the MHD solutions (dashed grey lines) at low σ

Finally, figure 8 presents a series of plots similar to figure 7(d), for various values of $\theta_1 \in [0, \pi/2].$

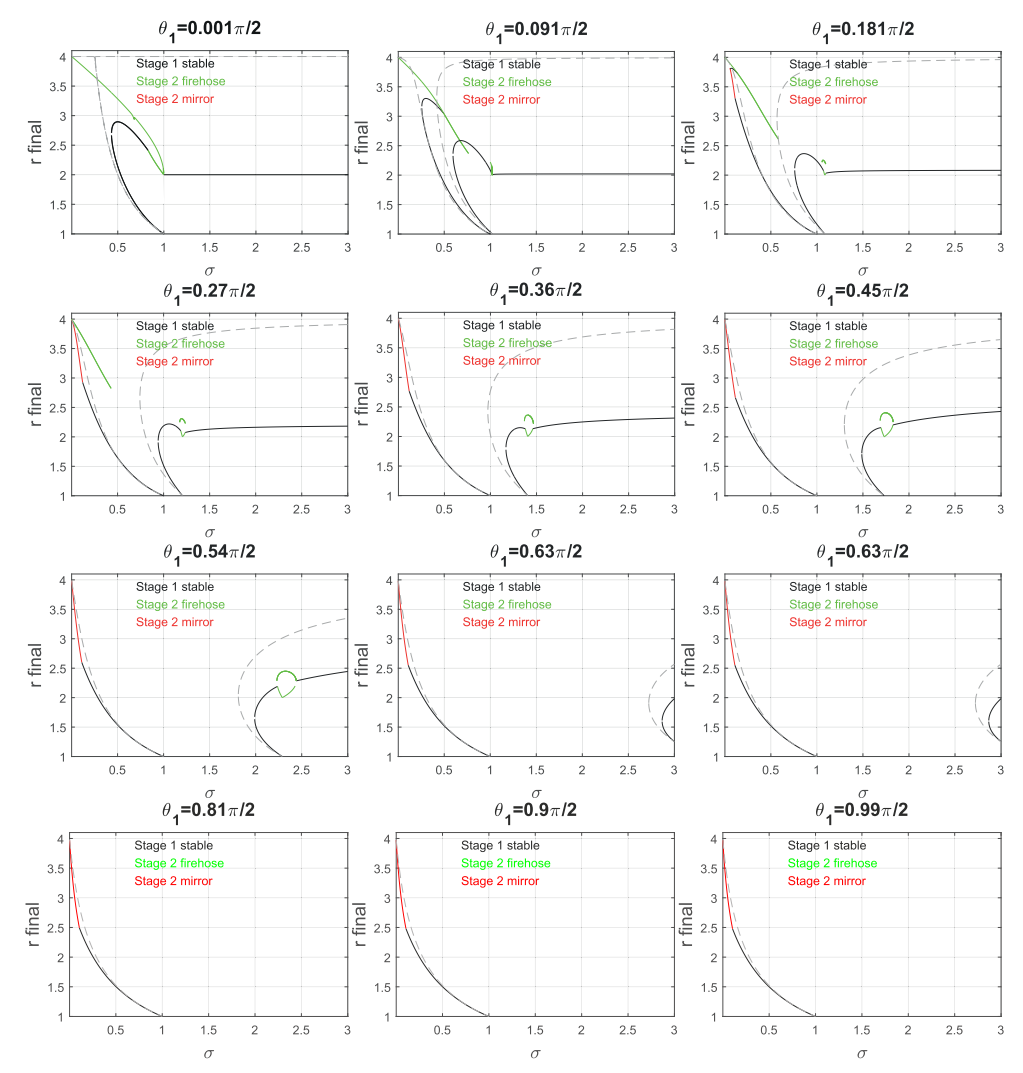


FIGURE 8. Similar to figure 7(*d*), but for various values of $\theta_1 \in [0, \pi/2]$. The grey dashed lines show the MHD solutions.

8. Conclusion

In a series of recent articles, we elaborated a model of collisionless shocks. Having treated the parallel, the perpendicular and the switch-on cases (Bret & Narayan 2018, 2019, 2022), with our model for the parallel case being successfully tested against PIC simulations (Haggerty *et al.* 2022), we here treated the general oblique case.

The MHD conservation equations for the general oblique case tend to be involved. The MHD conservation equations for anisotropic temperatures are even more involved. And our model adds temperature prescriptions to these equations. As a result, its resolution is lengthy and requires extensive use of Mathematica, to symbolically derive the key equations, and of MATLAB, to numerically solve them. The present work was devoted to the exposition of the mathematical solutions offered by our model. Their physics will be assessed in a forthcoming article.

In this respect, our model frequently offers various solutions for the same value of σ . Yet, figure 5(a,c) shows that such is also the case in MHD. This is also visible in figure 7(a-d) and in most of figure 8. In MHD, the solution selected depends on its physical relevance (see second-to-last paragraph of the introduction), or on the initial conditions of the shock formation like, for example, which initial states of a Riemann problem it is supposed to connect. In general, this second issue, namely connecting two different states, requires a succession of shocks rather than one single shock (see e.g. Ryu & Jones 1995). In our model, the choice of the solution when various are offered will most probably depend on the same factors. This topic will be addressed in a forthcoming paper.

Even though only the case of a cold upstream has been solved here, the formalism allows in principle for an anisotropic upstream.

Although we treated the field obliquity as an arbitrary parameter, this study remains limited in various ways:

- (a) A pair plasma is considered.
- (b) Velocities are non-relativistic.
- (c) The upstream pressure is assumed zero.
- (d) The shock is coplanar, namely upstream and downstream fields and velocities share a common plane.

Regarding limitation (a), PIC simulations could be used to test the relevance of our model to electron-ion plasmas, provided the σ parameter in (3.9a-c) is defined using the ion mass.

Tackling the other limitations altogether is clearly out of reach. At any rate, further testing of our model is envisioned through PIC simulations or comparison with in situ measurements at interplanetary shocks, by spacecrafts like Advanced Composition Explorer, Wind or the Parker Solar Probe (see e.g. David et al. 2022).

As evidenced in figure 8, deviations from MHD are more pronounced for quasi-parallel shocks and $\sigma > 1$. This is therefore the domain where our model should preferably be compared with PIC simulations or in situ measurements.

Acknowledgements

Thanks are due to Roberto Piriz for enriching discussions.

Editor Luís O. Silva thanks the referees for their advice in evaluating this article.

Funding

A.B. acknowledges support from the Ministerio de Economía y Competitividad of Spain (Grant No. PID2021-125550OB-I00). R.N. acknowledges support from NSF Grant No. AST-1816420. R.N. and A.B. thank the Black Hole Initiative at Harvard University for support. The BHI is funded by grants from the John Templeton Foundation and the Gordon and Betty Moore Foundation.

Declaration of interests

The authors report no conflict of interest.

REFERENCES

BALE, S.D., KASPER, J.C., HOWES, G.G., QUATAERT, E., SALEM, C. & SUNDKVIST, D. 2009 Magnetic fluctuation power near proton temperature anisotropy instability thresholds in the solar wind. Phys. Rev. Lett. 103, 211101.

- BEREZHKO, E.G. & ELLISON, D. C. 1999 A simple model of nonlinear diffusive shock acceleration. *Astrophys. J.* **526** (1), 385–399.
- BRET, A. 2010 Transferring a symbolic polynomial expression from *Mathematica* to *Matlab*. arXiv:1002.4725.
- BRET, A. 2020 Can we trust MHD jump conditions for collisionless shocks? Astrophys. J. 900 (2), 111.
- BRET, A. & NARAYAN, R. 2018 Density jump as a function of magnetic field strength for parallel collisionless shocks in pair plasmas. *J. Plasma Phys.* **84** (6), 905840604.
- BRET, A. & NARAYAN, R. 2019 Density jump as a function of magnetic field for collisionless shocks in pair plasmas: the perpendicular case. *Phys. Plasmas* **26** (6), 062108.
- Bret, A. & Narayan, R. 2020 Density jump for parallel and perpendicular collisionless shocks. *Laser Part. Beams* **38** (2), 114–120.
- BRET, A. & NARAYAN, R. 2022 Density jump as a function of magnetic field for switch-on collisionless shocks in pair plasmas. *J. Plasma Phys.* **88** (3), 905880320.
- CHEW, G.F., GOLDBERGER, M.L. & LOW, F.E. 1956 The Boltzmann equation and the one-fluid hydromagnetic equations in the absence of particle collisions. *Proc. R. Soc. Lond.* A **236** (1204), 112–118.
- DAVID, L., FRASCHETTI, F., GIACALONE, J., WIMMER-SCHWEINGRUBER, R.F., BERGER, L. & LARIO, D. 2022 In situ measurement of the energy fraction in suprathermal and energetic particles at ACE, wind, and PSP interplanetary shocks. *Astrophys. J.* **928** (1), 66.
- DELMONT, P. & KEPPENS, R. 2011 Parameter regimes for slow, intermediate and fast MHD shocks. *J. Plasma Phys.* 77 (2), 207–229.
- ERKAEV, N.V., VOGL, D.F. & BIERNAT, H.K. 2000 Solution for jump conditions at fast shocks in an anisotropic magnetized plasma. *J. Plasma Phys.* **64**, 561–578.
- FALLE, S.A.E.G. & KOMISSAROV, S.S. 1997 On the Existence of Intermediate Shocks. In *Computational Astrophysics; 12th Kingston Meeting on Theoretical Astrophysics* (ed. D.A. Clarke & M.J. West), Astronomical Society of the Pacific Conference Series, vol. 12, p. 66.
- FELDMAN, W.C., BAME, S.J., GARY, S.P., GOSLING, J.T., MCCOMAS, D., THOMSEN, M.F., PASCHMANN, G., SCKOPKE, N., HOPPE, M.M. & RUSSELL, C.T. 1982 Electron heating within the earth's bow shock. *Phys. Rev. Lett.* **49** (3), 199–201.
- GARY, S.P. 1993 Theory of Space Plasma Microinstabilities. Cambridge University Press.
- GARY, S.P. & KARIMABADI, H. 2009 Fluctuations in electron-positron plasmas: linear theory and implications for turbulence. *Phys. Plasmas* 16 (4), 042104.
- GÉNOT, V. 2009 Analytical solutions for anisotropic MHD shocks. *Astrophys. Space Sci. Trans.* **5** (1), 31–34.
- GOEDBLOED, J.P. 2008 Time reversal duality of magnetohydrodynamic shocks. *Phys. Plasmas* **15** (6), 062101.
- GOEDBLOED, J.P., KEPPENS, R. & POEDTS, S. 2010 Advanced Magnetohydrodynamics: With Applications to Laboratory and Astrophysical Plasmas. Cambridge University Press.
- GUO, X., SIRONI, L. & NARAYAN, R. 2017 Electron heating in low-Mach-number perpendicular shocks. I. Heating mechanism. *Astrophys. J.* **851**, 134.
- GUO, X., SIRONI, L. & NARAYAN, R. 2018 Electron heating in low mach number perpendicular shocks. II. Dependence on the pre-shock conditions. *Astrophys. J.* **858**, 95.
- GURNETT, D.A. & BHATTACHARJEE, A. 2005 Introduction to Plasma Physics: With Space and Laboratory Applications. Cambridge University Press.
- HAGGERTY, C.C., BRET, A. & CAPRIOLI, D. 2022 Kinetic simulations of strongly magnetized parallel shocks: deviations from MHD jump conditions. *Mon. Not. R. Astron. Soc.* **509** (2), 2084–2090.
- HASEGAWA, A. 1975 *Plasma Instabilities and Nonlinear Effects*. Springer Series on Physics Chemistry Space, vol. 8. Springer.
- HUDSON, P.D. 1970 Discontinuities in an anisotropic plasma and their identification in the solar wind. *Planet. Space Sci.* **18** (11), 1611–1622.
- KENNEL, C.F., BLANDFORD, R.D. & WU, C.C. 1990 Structure and evolution of small-amplitude intermediate shock waves. *Phys. Fluids* B **2** (2), 253–269.
- KULSRUD, R.M. 2005 Plasma Physics for Astrophysics. Princeton University Press.
- LANDAU, L.D. & LIFSHITZ, E.M. 1981 Course of Theoretical Physics, Physical Kinetics, vol. 10. Elsevier.

- MARUCA, B.A., KASPER, J.C. & BALE, S.D. 2011 What are the relative roles of heating and cooling in generating solar wind temperature anisotropies? Phys. Rev. Lett. 107, 201101.
- RYU, D. & JONES, T.W. 1995 Numerical magnetohydrodynamics in astrophysics: algorithm and tests for one-dimensional flow. Astrophys. J. 442, 228.
- SCHLICKEISER, R., MICHNO, M.J., IBSCHER, D., LAZAR, M. & SKODA, T. 2011 Modified temperature-anisotropy instability thresholds in the solar wind. Phys. Rev. Lett. 107, 201102.
- SILVA, T., AFEYAN, B. & SILVA, L.O. 2021 Weibel instability beyond bi-Maxwellian anisotropy. Phys. *Rev.* E **104** (3), 035201.
- THORNE, K.S. & BLANDFORD, R.D. 2017 Modern Classical Physics: Optics, Fluids, Plasmas, Elasticity, Relativity, and Statistical Physics. Princeton University Press.
- WEIBEL, E.S. 1959 Spontaneously growing transverse waves in a plasma due to an anisotropic velocity distribution. Phys. Rev. Lett. 2, 83.
- Wu, C.C. 2003 MKDVB and CKB Shock Waves. Space Sci. Rev. 107 (1), 403-421.